HHS Public Access

Author manuscript

Epilepsia. Author manuscript; available in PMC 2017 June 01.

Published in final edited form as:

Epilepsia. 2016 June ; 57(6): 977–983. doi:10.1111/epi.13376.

Hilar somatostatin interneuron loss reduces dentate gyrus inhibition in a mouse model of temporal lobe epilepsy

Gabrielle Hofmann[1,2], **Laura Balgooyen**[1,3], **Joanna Mattis**[4,5], **Karl Deisseroth**[4,5], and **Paul S. Buckmaster**[1,6]

[1]Department of Comparative Medicine, Stanford University, Stanford, California 94305

[2]College of Veterinary Medicine, University of Illinois at Urbana-Champaign, Urbana, Illinois 61802

[3]College of Veterinary Medicine, Michigan State University, East Lansing, Michigan 48824

[4]Department of, Bioengineering, Stanford University, Stanford, California 94305

[5]Department of Psychiatry & Behavioral Sciences, Stanford University, Stanford, California 94305

[6]Department of Neurology & Neurological Sciences, Stanford University, Stanford, California 94305

Summary

Objective—In patients with temporal lobe epilepsy, seizures usually start in the hippocampus, and dentate granule cells are hyperexcitable. Somatostatin interneurons are a major subpopulation of inhibitory neurons in the dentate gyrus, and many are lost in patients and animal models. However, surviving somatostatin interneurons sprout axon collaterals and form new synapses, so the net effect on granule cell inhibition remains unclear.

Methods—The present study uses optogenetics to activate hilar somatostatin interneurons and measure the inhibitory effect on dentate gyrus perforant path evoked local field potential responses in a mouse model of temporal lobe epilepsy.

Results—In controls, light activation of hilar somatostatin interneurons inhibited evoked responses up to 40%. Epileptic pilocarpine-treated mice exhibited loss of hilar somatostatin interneurons and less light-induced inhibition of evoked responses.

Significance—These findings suggest that severe epilepsy-related loss of hilar somatostatin interneurons can overwhelm the surviving interneurons' capacity to compensate by sprouting axon collaterals.

Corresponding author. Paul Buckmaster, 300 Pasteur Drive, R321 Edwards Building, Department of Comparative Medicine, Stanford University, Stanford, CA 94305, (650)498-4774, (650)498-5085 (fax), psb@stanford.edu.

Disclosure of Conflicts of Interest

None of the authors has any conflict of interest to disclose.

We confirm that we have read the Journal's position on issues involved in ethical publication and affirm that this report is consistent with those guidelines.

Keywords

dentate gyrus; perforant path; hippocampus; optogenetics; channelrhodopsin; local field potential; pilocarpine; C57BL/6J mice

Introduction

In patients with temporal lobe epilepsy, seizures usually start in the hippocampus[1], where hilar neuron loss is common[2]. Somatostatin-expressing GABAergic interneurons are abundant in the hilus, but many of these interneurons are lost in patients with temporal lobe epilepsy[3] and in animal models[4]. Individual somatostatin-positive interneurons make profuse inhibitory synapses with granule cells[5]. Therefore, epilepsy-related loss of hilar somatostatin interneurons would be expected to reduce inhibition in the dentate gyrus. However, surviving somatostatin interneurons sprout axons[6] and form new synapses with granule cells[7,8]. Consequently, the net functional effect of initial loss and subsequent recovery of GABAergic input from hilar somatostatin interneurons to granule cells remains unclear. To address this question, we used optogenetics to activate hilar somatostatin interneurons and measure their inhibitory effect in the dentate gyrus of an animal model of temporal lobe epilepsy.

Methods

All animal procedures were conducted in accordance with the National Institutes of Health *Guide for the Care and Use of Laboratory Animals* and approved by an institutional animal care and use committee at Stanford University. Animals used were homozygous somatostatin-Flp mice[9], which are now commercially available ($Sst^{tm3.1(flop)Zjh}$/J, stock number 028579, Jackson Laboratories). The mice are on the C57BL/6J background, which is resistant to developing pilocarpine-induced epilepsy[10]. In pilot experiments, other protocols were tested, but the following was most reliable at generating epileptic mice. Mice received 5 mg/kg atropine methyl bromide (intraperitoneally, i.p.) and 20 min later 275 mg/kg pilocarpine (i.p.) to induce status epilepticus. After 2 h of status epilepticus they received 5 mg/kg diazepam (i.p.). For up to a week, they were kept warm with a heating pad and received lactated Ringer's (subcutaneously, s.c.) to maintain hydration. A total of 961 mice were treated with pilocarpine. In response, 42% failed to develop status epilepticus, 54% developed status epilepticus and died, and 4% developed status epilepticus and survived. Data were obtained from male (n=33) and female (n=25) mice that had been treated with pilocarpine when they were 42 ± 2 d old (mean ± s.e.m.). Controls had been treated with pilocarpine but did not develop status epilepticus. To test whether the protocol caused epilepsy, limited video monitoring was performed for spontaneous seizures beginning at least 7 d after pilocarpine treatment. Seizures of grade 3 or greater[11] were observed in 24/29 mice that experienced status epilepticus. No seizures were observed in controls (n=29).

One month after pilocarpine treatment, a Flp-dependent recombinant adeno-associated virus (AAV) vector was injected into the right hippocampus. Mice were anesthetized (3% isoflurane) and placed in a stereotaxic apparatus. Analgesic was administered (5 mg/kg

carprofen, s.c.), bupivacaine (0.25%) was injected along the midline of the scalp (s.c.), and the site was prepared for aseptic surgery. Holes were drilled in the skull for a recording electrode (1.8 mm posterior, 1.4 mm right of bregma) and a stimulating electrode (4.0 mm posterior, 3.6 mm right). A bipolar electrode was lowered ~1.2 mm below the brain surface to stimulate the perforant path. Bipolar electrodes consisted of 25 μm diameter insulated stainless steel wires with 1 mm tip separation. Local field potential recordings were obtained with a ~15 μm tip diameter glass electrode containing 0.9% NaCl. These recordings were amplified (AxoClamp-2B, CyberAmp 380, Molecular Devices), visualized (pClamp, Molecular Devices), and used to identify the depth of the hilus based on waveform[12]. Viral vector consisted of 3.2×10^{13} genomes/mL of rAAV5/Ef1a-fDIO-ChR2(H134R)-EYFP[9] dialyzed with 350 mM NaCl and 5% D-sorbitol in phosphate buffered saline (University of North Carolina Vector Core) diluted 1:10. Vector was injected into the hilus at 100 nL/min for 10 min with a 33 gauge needle and microsyringe pump controller (World Precision Instruments). After another 10 min, the needle was slowly retracted, the skin was sutured, and the mouse recovered.

One month after viral vector injection, mice were anesthetized (3% isoflurane), placed in a stereotaxic apparatus, and prepared for perforant path stimulation and dentate gyrus field potential recording. A 300 μm diameter optic fiber (Thor Labs) was attached to the recording electrode. The tip of the field potential electrode extended 1 mm deeper than the tip of the optic fiber. The optic fiber was coupled to a 447 nm diode-pumped solid-state laser (Dragon Lasers). Pilot experiments yielded a light stimulus protocol that inhibited dentate gyrus field potentials. The light stimulus consisted of train a brief pulses (2 ms duration, 100 mW, 33 Hz) that began 20 ms before perforant path stimulation and lasted 25 ms. The perforant path was stimulated (150 μs duration) once every 15 s. Stimulus intensity was gradually increased to identify the population spike threshold (T). Perforant path stimulus intensity was set at 0.75xT, and 10 trials were recorded with the laser off, followed by 10 with the laser on, then another 10 with the laser off, and finally 10 with the laser on but perforant path stimulation off. The process was repeated with stimulus intensity set at 1.5xT. Local field potential responses of trials were averaged, and the amplitude of the field excitatory postsynaptic potential (fEPSP) with and without light activation was measured from prestimulus baseline to peak. The amplitude of the population spike was measured from the fEPSP immediately before the onset of the population spike to the most negative value of the population spike. Percent inhibition was calculated as 100 × (amplitude with laser off − amplitude with laser on) / (amplitude with laser off).

Immediately after recording, mice were killed (>100 mg/kg pentobarbital, i.p.) and perfused through the ascending aorta at 15 mL/min for 1 min with 0.9% NaCl, 5 min with 0.37% sodium sulfide, 1 min with 0.9% NaCl, and 30 min with 4% formaldehyde in 0.1 M phosphate buffer (PB, pH 7.4). Brains post-fixed overnight at 4°C. The right hippocampus was isolated, cryoprotected in 30% sucrose in 0.1 M PB, frozen, and stored at −80°C. Later, hippocampi were thawed, slightly straightened, frozen, and sectioned from the septal pole to the temporal pole with a sliding microtome set at 40 μm.

Beginning at a random point near the septal pole, series of adjacent sections were processed for Nissl staining (1-in-12 sections), Timm staining (1-in-24), somatostatin-

immunoreactivity (1-in-12), green fluorescent protein (GFP)-immunoreactivity (1-in-6), and double-labeling for vector-expressed enhanced yellow fluorescent protein (EYFP) and somatostatin-immunoreactivity (1-in-24). Established protocols were used for Nissl and Timm staining[13]. Immunostaining protocols were similar to those published previously[7], except sections were exposed to primary antibodies for 7 d at 4°C. Primary antibodies included a polyclonal rabbit anti-somatostatin serum (1:16,000, T-4130, Peninsula Laboratories) and a polyclonal rabbit anti-GFP serum that cross reacts with EYFP (1:20,000, Invitrogen). The optical fractionator method was used as published previously[7] to estimate numbers of somatostatin- and GFP-immunoreactive interneurons per dentate gyrus.

To compare control and epileptic groups, a two-tailed t test was used (SigmaPlot 12, Systat), which assumes samples were drawn from normally distributed populations with equal variances. The Shapiro-Wilk test was used to measure normality. Equal variance was tested by checking the variability about the group means. If normality or equal variance tests failed, a Mann-Whitney rank sum test or Wilcoxin signed rank test was used. Differences were considered significant if $p<0.05$. Results are reported as mean ± s.e.m.

Results

To test whether mice developed neuropathology similar to that of patients with temporal lobe epilepsy, Nissl- and Timm-stained hippocampal sections were evaluated. All epileptic mice displayed obvious neuron loss in the hilus. Additionally, 86% (25/29) displayed obvious neuron loss in CA3, and 66% (19/29) displayed obvious neuron loss in CA1 (Figure 1AB). Granule cells, CA2 pyramidal cells, and subicular neurons appeared to be spared. All epileptic mice displayed aberrant, black Timm staining in the inner molecular layer at all septotemporal levels of the hippocampus (Figure 1CD). These findings revealed that hippocampal neuron loss and synaptic reorganization is similar in the epileptic pilocarpine-treated mice and human patients with temporal lobe epilepsy[2,14].

To test whether epileptic mice displayed somatostatin interneuron loss, immunocytochemistry was used. Somatostatin interneurons in the dentate gyrus were largely confined to the hilus. Hilar somatostatin interneurons were more abundant in controls (Figure 1EF). Control mice had 1920 ± 60 somatostatin interneurons per dentate gyrus (Figure 1G). Epileptic mice had only 18% of controls (340 ± 40, $p<0.001$, t test). Somatostatin interneurons were more numerous in sections from the temporal part of the hippocampus (Figure 1H). Loss of somatostatin interneurons in epileptic mice occurred at all septotemporal levels and was almost complete in the septal half of the hippocampus.

To test for channelrhodopsin expression, GFP-immunocytochemistry was used. The viral vector included genes for channelrhodopsin and EYFP that were fused in-frame and co-expressed[15]. Therefore, expression levels of EYFP and channelrhodopsin might be correlated. GFP-immunoprocessing includes biotin-streptavidin amplification and better reveals fine anatomical details that are useful for identifying cell types. Cells were labeled with diaminobenzidine reaction product, facilitating quantification by our stereological software and hardware. In control mice GFP-positive somata and dendrites were abundant in the hilus of the dentate gyrus (Figure 2AC). Somata were round or oval, dendrites were thin,

even where they attached to the soma, and long simple spines were most dense distally. Occasional GFP-positive dendrites extended through the granule cell layer and into the molecular layer. GFP-positive axons extended through the granule cell layer and ramified extensively in the molecular layer. Some collaterals extended into stratum radiatum and stratum lacunosum-moleculare of CA3 and near the border of those strata in CA1. Similar characteristics have been reported for hilar somatostatin interneurons[5,7,16]. GFP-immunoreactivity also was evident in some cells with morphological characteristics of granule cells, but most were only faintly labeled.

Transfected cells would be expected to express GFP and be located near the site of viral vector injection, which was approximately 25% of the septotemporal distance from the septal pole of the hippocampus. GFP-positive hilar neurons were most abundant in the septal two-thirds of the hippocampus (Figure 2F). The broad septotemporal span of transfected hilar neurons might be attributable to spread of the viral vector from the injection site. The long, septotemporally projecting axons of hilar somatostatin interneurons[5] also might be responsible. At 25% of the septotemporal distance from the septal pole, the number of GFP-positive neuron profiles was 68% of the number of somatostatin profiles. Therefore, most of the hilar somatostatin interneurons near the viral vector injection site were transfected.

Epileptic mice displayed fewer GFP-positive hilar neurons than controls (Figure 2BD). Control mice had 424 ± 33 GFP-positive hilar neurons per dentate gyrus (Figure 2E). Epileptic mice had only 9% of controls (37 ± 6, $p<0.001$, Mann-Whitney rank sum test). In epileptic mice, numbers of GFP-positive hilar neurons were reduced at all septotemporal levels. These findings suggested that epileptic mice had fewer GFP-positive hilar neurons because they had fewer surviving somatostatin interneurons. Alternatively, viral vector injections might have been misplaced in epileptic animals, which seemed unlikely because injection sites were determined by hilar electrophysiological characteristics. Nevertheless, to test that possibility, GFP-positive neurons in the granule cell layer were counted even if only weakly labeled as a measure of injection site accuracy. There was no significant difference in the number of GFP-positive neurons in the granule cell layer per dentate gyrus of control (1520 ± 150) and epileptic mice (1190 ± 110), suggesting vector injections were similarly placed in both groups.

To test whether EYFP-expressing neurons were somatostatin interneurons, sections were labeled for fluorescent somatostatin-immunoreactivity (Figure 3). As expected, fewer cells were detected by EYFP expression than with GFP-immunocytochemistry. Of the 197 EYFP-positive hilar neurons identified, 192 (97%) were somatostatin-immunoreactive. Only 43 EYFP-positive cells were found in the granule cell layer, and only 2 of those (5%) were somatostatin-immunoreactive. Thus, 194/240 (81%) of the cells expressing detectable levels of EYFP were somatostatin-positive. Those cells were most likely to be expressing functional levels of channelrhodopsin.

To test the functional effect of hilar somatostatin interneurons, they were activated by light beginning 20 ms before stimulating the perforant path, which is the predominant excitatory input to granule cells[12]. Local field potentials were recorded in the hilus. Perforant path stimulation at 0.75xT evoked similar local field potential waveforms in the control and

epileptic mice (Figure 4AB). Without light, fEPSP amplitudes were similar in control (3.0 ± 0.3 mV) and epileptic mice (2.8 ± 0.5 mV). With light, in controls fEPSP amplitudes were substantially reduced (1.9 ± 0.2 mV, $p<0.001$, paired t test) by 40.0 ± 4.4%. In epileptic mice, light stimulation reduced fEPSP amplitudes (2.5 ± 0.5 mV, $p<0.001$, Wilcoxin signed rank test) but only by 9.9 ± 2.8%. Light-induced inhibition of fEPSP amplitude was greater in control versus epileptic mice ($p<0.001$, Mann-Whitney rank sum test) (Figure 4E). Light stimulation alone evoked virtually no change in the field potential.

Perforant path stimulation at 1.5xT evoked a population spike in control and epileptic mice (Figure 4CD). To be included for analysis, population spike amplitude had to be >2 mV, and 3 epileptic animals did not meet that criterion. Without light, population spike amplitudes were similar in control (11.8 ± 1.4 mV) and epileptic mice (9.2 ± 0.8 mV). With light, population spike amplitudes were significantly reduced in both control (9.8 ± 1.5 mV, $p<0.001$, Wilcoxin signed rank test) and epileptic mice (8.9 ± 0.9 mV, $p=0.035$, Wilcoxin signed rank test). Light-induced percent inhibition of population spike amplitude was over 5X greater in control (20.5 ± 4.2%) versus epileptic mice (3.9 ± 1.8%; $p=0.004$, Mann-Whitney rank sum test) (Figure 4F).

Discussion

The principal findings of the present study were that optogenetic activation of hilar somatostatin interneurons inhibited local field potential responses to perforant path stimulation, and inhibition was reduced in epileptic pilocarpine-treated mice with somatostatin interneuron loss.

Evidence suggested that light-induced inhibition of perforant path responses was mediated by hilar somatostatin neurons. Somatostatin interneurons were targeted by injecting a Flp-recombinase-dependent virus (Flp is analogous to Cre) into the hilus of a mouse line in which Flp-recombinase is expressed in somatostatin interneurons. Viral vector injection sites were electrophysiologically localized to the hilus. GFP-expression was most extensive in the dentate gyrus. EYFP expression was most abundant in hilar neurons, and 81% of EYFP-positive neurons were somatostatin-positive. Although some granule cells and some neurons outside of the dentate gyrus were GFP-positive, results suggested the greatest expression of channelrhodopsin was by hilar somatostatin interneurons. Thus, although optogenetic excitation was not strictly limited to hilar somatostatin interneurons, those interneurons were the most likely generators of light-induced inhibition of perforant path evoked responses.

Inhibition of perforant path evoked responses by optogenetically activating hilar somatostatin interneurons is consistent with previous findings. In rats[17] and monkeys[18] somatostatin interneurons account for one-quarter of all GABAergic interneurons in the dentate gyrus, and more than half of those in the hilus. Axon projections of individual hilar somatostatin interneurons span over half the septotemporal length of the hippocampus and make profuse inhibitory synapses with granule cell dendrites, many on spines that receive excitatory input[5]. Unitary inhibitory postsynaptic responses of hilar somatostatin-to-granule cell synapses are strong[7]. Therefore, it was not surprising that optogenetic activation of hilar somatostatin interneurons inhibited perforant path evoked responses in control animals.

Why did epileptic mice display so little somatostatin-mediated inhibition? Recordings were obtained 2 months after status epilepticus, which is sufficient for somatostatin axons to sprout and form functional inhibitory synapses with granule cells[7]. After an initial drop following status epilepticus-induced neuron loss, the number of GABAergic synapses with granule cell dendrites recovers and overshoots control values[8]. Somatostatin interneurons in CA1 also sprout axons into the dentate gyrus molecular layer[19], but CA1 interneurons were not optogenetically targeted in the present study. In epileptic mice, numbers of hilar somatostatin interneurons were reduced to only 18% of controls, which is more severe loss than is typically found in kainate-treated rats[4] and pilocarpine-treated mice of the FVB strain[7]. The extensive hilar somatostatin neuron loss did not appear to be attributable to infection by viral vector because it also occurred outside the vector injection site. Furthermore, CA3 and CA1 pyramidal cell loss also was more severe than in previous studies. Together, these findings suggest that epilepsy related hippocampal neuron loss was severe in mice of the present study, and that the capacity for potentially compensatory axon sprouting by surviving hilar somatostatin interneurons was limited by extensive loss of interneurons. Additional studies of epileptic animals with less severe hilar somatostatin interneuron loss would be necessary to evaluate the effects of sprouting.

Hilar somatostatin interneuron loss can be similarly extensive in patients with temporal lobe epilepsy[3,6]. Therefore, it is possible that patients experience reduced hilar somatostatin interneuron-mediated inhibition of dentate granule cells similar to that in the present study. However, more work is needed to clarify the extent to which this loss is compensated by other sources and mechanisms.

Acknowledgments

Supported by NINDS and the Office of the Director of NIH. The authors are grateful to Yui Yin Chu and Dr. Xiling Wen for technical assistance and to Emily Abrams for technical and editorial assistance.

References

1. Quesney LF. Clinical and EEG features of complex partial seizures of temporal lobe origin. Epilepsia. 1986; 27(suppl 2):S27–S45. [PubMed: 3720711]
2. Margerison JH, Corsellis JA. Epilepsy and the temporal lobes. Brain. 1966; 89:499–530. [PubMed: 5922048]
3. de Lanerolle NC, Kim JH, Robbins RJ, et al. Hippocampal interneuron loss and plasticity in human temporal lobe epilepsy. Brain Res. 1989; 495:387–395. [PubMed: 2569920]
4. Buckmaster PS, Dudek FE. Neuron loss, granule cell axon reorganization, and functional changes in the dentate gyrus of epileptic kainate-treated rats. J Comp Neurol. 1997; 385:385–404. [PubMed: 9300766]
5. Buckmaster PS, Yamawaki R, Zhang GF. Axon arbors and synaptic connections of a vulnerable population of interneurons in the dentate gyrus in vivo. J Comp Neurol. 2002; 445:360–373. [PubMed: 11920713]
6. Mathern GW, Babb TL, Pretorius JK, et al. Reactive synaptogenesis and neuron densities for neuropeptide Y, somatostatin, and glutamate decarboxylase immunoreactivity in the epileptogenic human fascia dentata. J Neurosci. 1995; 15:3990–4004. [PubMed: 7751960]
7. Zhang W, Yamawaki R, Wen X, et al. Surviving hilar somatostatin interneurons enlarge, sprout axons, and form new synapses with granule cells in a mouse model of temporal lobe epilepsy. J Neurosci. 2009; 29:14247–14256. [PubMed: 19906972]

8. Thind KK, Yamawaki R, Phanwar I, et al. Initial loss but later excess of GABAergic synapses with dentate granule cells in a rat model of temporal lobe epilepsy. J Comp Neurol. 2010; 518:647–667. [PubMed: 20034063]
9. Fenno LE, Mattis J, Ramakrishnan C, et al. Targeting cells with single vectors using multiple-feature Boolean logic. Nat Methods. 2014; 11:763–772. [PubMed: 24908100]
10. Borges K, Gearing M, McDermott DL, et al. Neuronal and glial pathological changes during epileptogenesis in the mouse pilocarpine model. Exp Neurol. 2003; 182:21–34. [PubMed: 12821374]
11. Racine RJ. Modification of seizure activity by electrical stimulation. II. Motor seizure. Electroencephalogr Clin Neurophysiol. 1972; 32:281–294. [PubMed: 4110397]
12. Andersen P, Holmqvist B, Voorhoeve PE. Entorhinal activation of dentate granule cells. Acta Physiol Scand. 1966; 66:448–460. [PubMed: 5927271]
13. Heng K, Haney MM, Buckmaster PS. High-dose rapamycin blocks mossy fiber sprouting but not seizures in a mouse model of temporal lobe epilepsy. Epilepsia. 2013; 54:1535–1541. [PubMed: 23848506]
14. Sutula T, Cascino G, Cavazos J, et al. Mossy fiber synaptic reorganization in the epileptic human temporal lobe. Ann Neurol. 1989; 26:321–330. [PubMed: 2508534]
15. Mattis J, Tye KM, Ferenczi EA, et al. Principles for applying optogenetic tools derived from direct comparative analysis of microbial opsins. Nat Methods. 2011; 9:159–172. [PubMed: 22179551]
16. Leranth C, Malcolm AJ, Frotscher M. Afferent and efferent synaptic connections of somatostatin-immunoreactive neurons in the rat fascia dentata. J Comp Neurol. 1990; 295:111–122. [PubMed: 1971287]
17. Buckmaster PS, Jongen-Rêlo AL. Highly specific neuron loss preserves lateral inhibitory circuits in the dentate gyrus of kainate-induced epileptic rats. J Neurosci. 1999; 19:9519–9529. [PubMed: 10531454]
18. Austin JE, Buckmaster PS. Recurrent excitation of granule cells with basal dendrites and low interneuron density and inhibitory postsynaptic current frequency in the dentate gyrus of macaque monkeys. J Comp Neurol. 2004; 476:205–218. [PubMed: 15269966]
19. Peng Z, Zhang N, Wei W, et al. A reorganized GABAergic circuit in a model of epilepsy: evidence from optogenetic labeling and stimulation of somatostatin interneurons. J Neurosci. 2013; 33:14392–14405. [PubMed: 24005292]

Key Point Box

- Optogenetic activation of hilar somatostatin interneurons inhibits evoked responses in the dentate gyrus.
- Epileptic pilocarpine-treated C57BL/6J mice display loss of hilar somatostatin interneurons.
- Epileptic mice exhibit reduced somatostatin interneuron-mediated inhibition in the dentate gyrus.

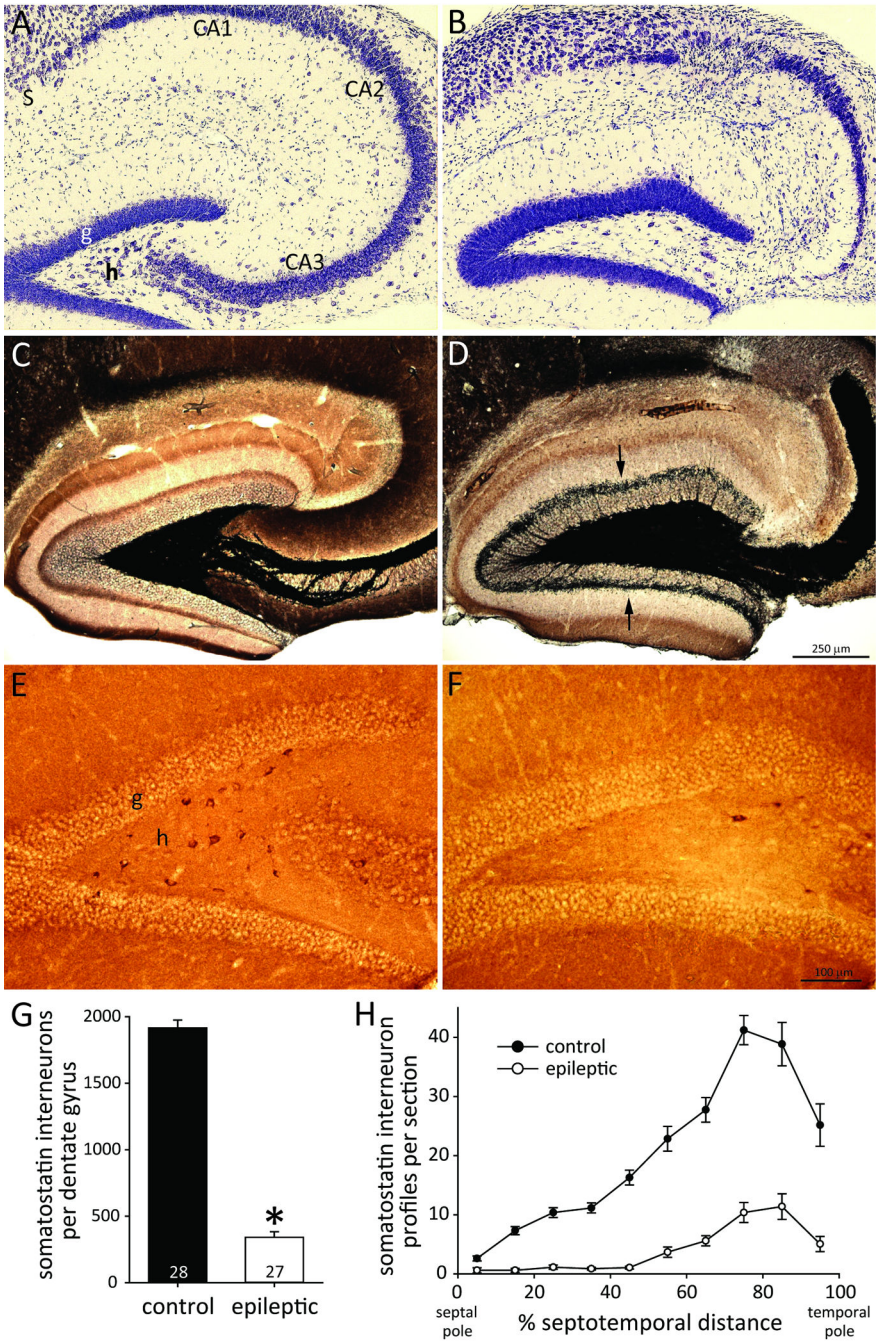

Figure 1.

Pilocarpine-treated C57BL/6J mouse model of temporal lobe epilepsy with loss of hilar somatostatin interneurons. Adjacent sections from the hippocampus in a control (**A,C,E**) and epileptic mouse (**B,D,F**). **A,B** Nissl-stained sections revealed loss of neurons in the hilus (h), CA3, and CA1 in the epileptic mouse. Neurons in the granule cell layer (g), CA2, and subiculum (S) appeared to be spared. **C,D** Timm staining revealed mossy fiber sprouting into the inner molecular layer in the epileptic mouse (arrows). **E,F** Somatostatin-immunoreactive neurons were numerous in the hilus of the control mouse but few remained

in the epileptic animal. **G** The average number of somatostatin interneurons per dentate gyrus was reduced in epileptic mice (*$p<0.001$). **H** Loss of somatostatin interneurons occurred at all septotemporal levels of the hippocampus in epileptic mice.

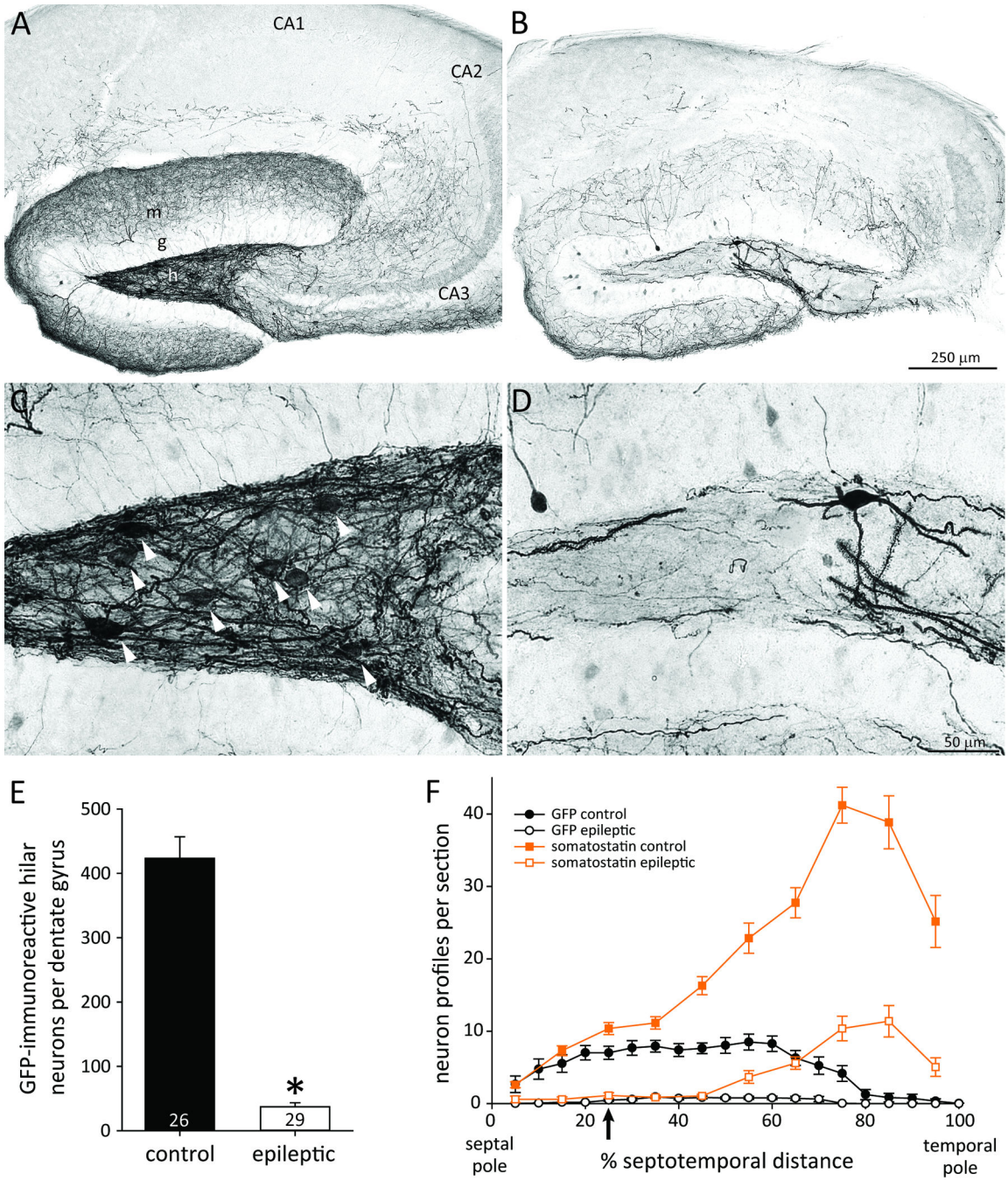

Figure 2.

GFP-immunoreactivity as a marker for channelrhodopsin in a control (**A,C**) and epileptic pilocarpine-treated mouse (**B,D**). **A,B** GFP-immunoreactivity was evident primarily in the dentate gyrus. m=molecular layer; g=granule cell layer; h=hilus. **C,D** Higher magnification revealed hilar GFP-positive neurons with somata (arrowheads in **C**) and spiny dendrites. **E** The average number of GFP-positive hilar neurons per dentate gyrus was reduced in epileptic mice (*p<0.001). **F** Loss of GFP-positive hilar neurons occurred at all septotemporal levels of the hippocampus in epileptic mice. For comparison, somatostatin

neuron profiles per section from Figure 1H also are plotted (squares and orange lines). The approximate site of virus injection, recording, and light stimulation is indicated (arrow).

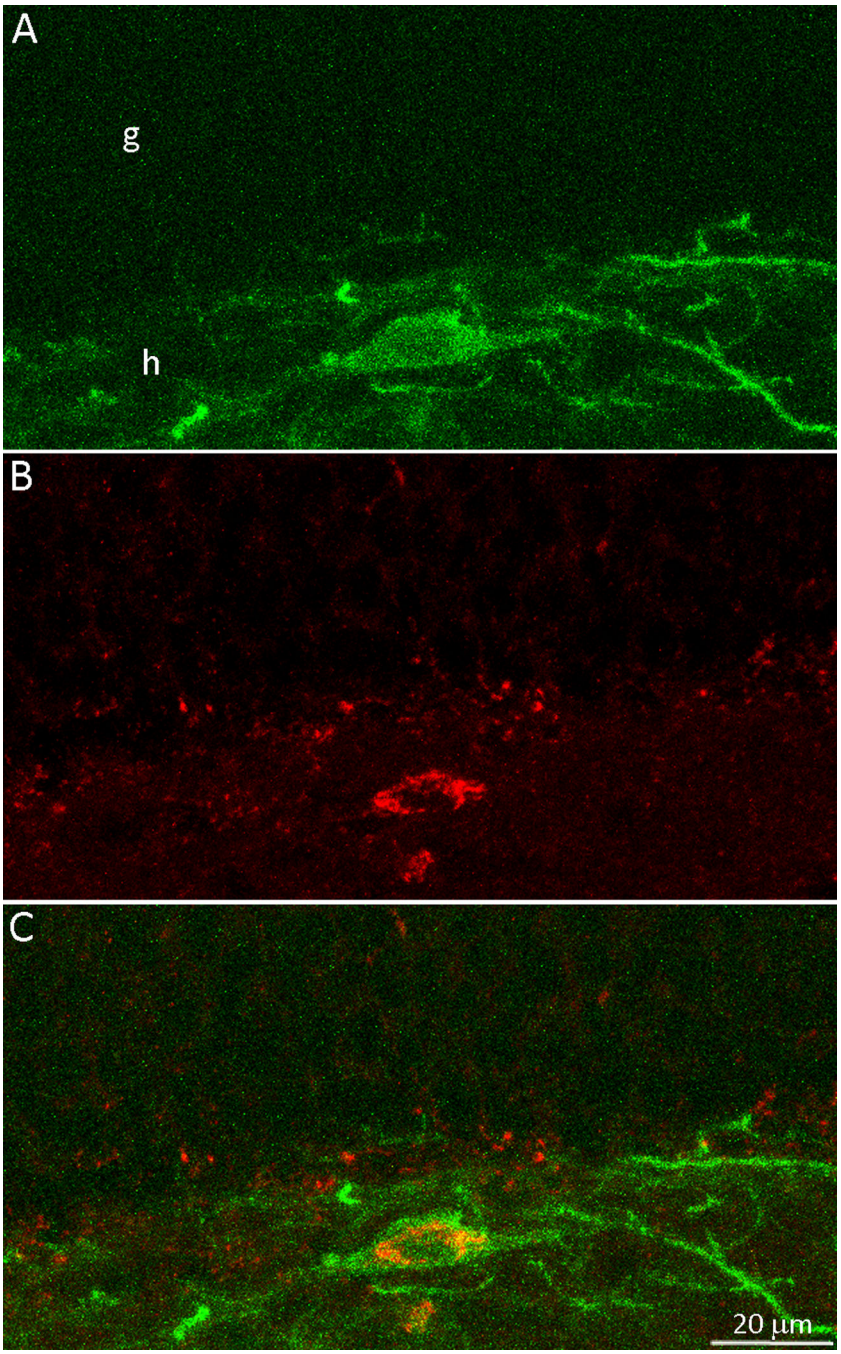

Figure 3.

Enhanced yellow fluorescent protein (EYFP) and somatostatin double-labeling in a control mouse. **A** A putative channelrhodopsin-positive neuron identified by EYFP. The green soma and dendrites were concentrated in the hilus (h). g=granule cell layer. **B** Immunocytochemistry for somatostatin revealed the red soma in the hilus. **C** The merged view revealed that the EYFP-positive hilar neuron was double-labeled for somatostatin.

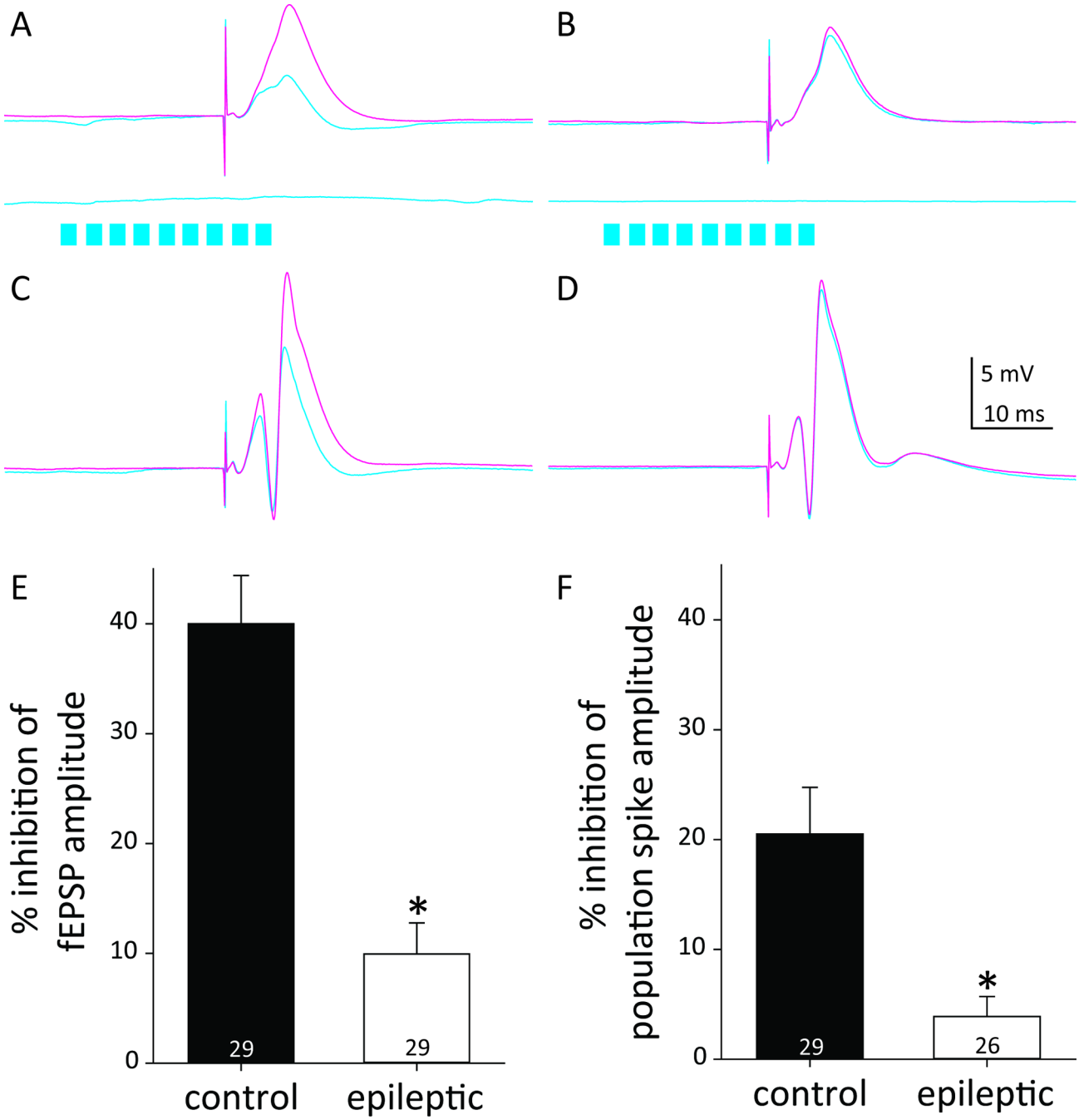

Figure 4.

Less inhibition in epileptic pilocarpine-treated mice. The perforant path was stimulated to excite the dentate gyrus, and responses were evaluated with and without optogenetic activation of hilar somatostatin interneurons. Local field potential responses recorded in the hilus of control (**A,C**) and epileptic mice (**B,D**). **A,B** Responses to stimulation at 0.75 × the intensity needed to evoke a population spike (T) without light (magenta) and with (cyan). Cyan traces below show responses to light activation (cyan bars) without perforant path stimulation. **C,D** Responses to stimulation at 1.5xT. **E** Light-induced percent inhibition of

fEPSP amplitude. *p<0.001. **F** Light-induced percent inhibition of population spike amplitude.